The Astrophysical Journal Letters, 825:L23 (6pp), 2016 July 10 doi:10.3847/2041-8205/825/2/L23

THE MOSDEF SURVEY: DETECTION OF [O III]λ4363 AND THE DIRECT-METHOD OXYGEN ABUNDANCE OF A STAR-FORMING GALAXY AT $z = 3.08$*

Ryan L. Sanders[1], Alice E. Shapley[1], Mariska Kriek[2], Naveen A. Reddy[3,6], William R. Freeman[3], Alison L. Coil[4], Brian Siana[3], Bahram Mobasher[3], Irene Shivaei[3], Sedona H. Price[2], and Laura de Groot[5]
[1] Department of Physics & Astronomy, University of California, Los Angeles, 430 Portola Plaza, Los Angeles, CA 90095, USA; rlsand@astro.ucla.edu
[2] Astronomy Department, University of California, Berkeley, CA 94720, USA
[3] Department of Physics & Astronomy, University of California, Riverside, 900 University Avenue, Riverside, CA 92521, USA
[4] Center for Astrophysics and Space Sciences, University of California, San Diego, 9500 Gilman Drive, La Jolla, CA 92093-0424, USA
[5] Department of Physics and Astronomy, Denison University, Granville, OH 43023, USA
Received 2016 June 13; revised 2016 June 15; accepted 2016 June 16; published 2016 July 8

ABSTRACT

We present measurements of the electron-temperature-based oxygen abundance for a highly star-forming galaxy at $z = 3.08$, COSMOS-1908. This is the highest redshift at which [O III]λ4363 has been detected and the first time that this line has been measured at $z > 2$. We estimate an oxygen abundance of $12 + \log(\mathrm{O/H}) = 8.00^{+0.13}_{-0.14}$. This galaxy is a low-mass ($10^{9.3}\ M_\odot$), highly star-forming ($\sim 50\ M_\odot\ \mathrm{yr}^{-1}$) system that hosts a young stellar population (~160 Myr). We investigate the physical conditions of the ionized gas in COSMOS-1908 and find that this galaxy has a high ionization parameter, little nebular reddening ($E(B-V)_{\mathrm{gas}} < 0.14$), and a high electron density ($n_e \sim 500\ \mathrm{cm}^{-3}$). We compare the ratios of strong oxygen, neon, and hydrogen lines to the direct-method oxygen abundance for COSMOS-1908 and additional star-forming galaxies at $z = 0 - 1.8$ with [O III]λ4363 measurements and show that galaxies at $z \sim 1$–3 follow the same strong-line correlations as galaxies in the local universe. This agreement suggests that the relationship between ionization parameter and O/H is similar for $z \sim 0$ and high-redshift galaxies. These results imply that metallicity calibrations based on lines of oxygen, neon, and hydrogen do not strongly evolve with redshift and can reliably estimate abundances out to $z \sim 3$, paving the way for robust measurements of the evolution of the mass–metallicity relation to high redshift.

Key words: galaxies: evolution – galaxies: high-redshift – galaxies: ISM

1. INTRODUCTION

The gas-phase metallicity of a galaxy is intimately connected to the processes governing galaxy formation and growth, namely, the fueling and regulation of star formation. This connection is observed as the mass–metallicity relation (MZR), a correlation between stellar mass (M_*) and gas-phase oxygen abundance for local star-forming galaxies (e.g., Tremonti et al. 2004; Andrews & Martini 2013). The MZR exists for high-redshift galaxies as well, and is observed to shift toward lower metallicity at fixed M_* out to $z \sim 3$ (e.g., Erb et al. 2006; Troncoso et al. 2014; Sanders et al. 2015; Onodera et al. 2016). Constraining the evolution of the shape and normalization of the MZR with redshift provides insight into how the interplay among star formation, gas accretion, and feedback changes over cosmic history. This approach requires robust estimates of the gas-phase metallicity at all epochs.

The ratio of the flux of the auroral [O III]λ4363 line to that of [O III]λλ4959, 5007 is sensitive to the electron temperature of the ionized gas. Based on estimates of the electron temperature and density, the oxygen abundance can be inferred from ratios of strong oxygen lines (e.g., [O III]λλ4959, 5007 and [O II]λ3727) to Balmer lines. Measurements of [O III]λ4363 have now been obtained for several hundred local H II regions and galaxies (e.g., Izotov et al. 2006; Marino et al. 2013). However, the direct electron-temperature-based method cannot be applied to the majority of local galaxies with spectroscopic observations because [O III]λ4363 is typically ~100 times weaker than [O III]λ5007 at low metallicity, and much weaker still at solar and higher abundances. For this reason, calibrations to determine metallicity from strong optical emission-line ratios have been constructed based on observations of H II regions and galaxies with direct metallicity measurements (e.g., Pettini & Pagel 2004; Pilyugin & Thuan 2005).

Strong-line calibrations have been widely applied at both low and high redshifts, but it is uncertain whether these local calibrations can accurately predict the metallicities of high-redshift galaxies. There is evidence that the physical conditions of the interstellar medium (ISM) in high-redshift galaxies differ from those observed locally. In order to explain offsets between $z \sim 0$ and high-redshift galaxies in diagnostic plots such as the [O III]/Hβ versus [N II]/Hα diagram, it has been proposed that high-redshift galaxies may have higher ionization parameters (Kewley et al. 2015; Cullen et al. 2016), harder ionizing stellar spectra (Steidel et al. 2014), higher density/ISM pressure (Kewley et al. 2013; Sanders et al. 2016), and/or anomalous nitrogen abundance at fixed O/H (Masters et al. 2014; Shapley et al. 2015; Sanders et al. 2016) compared to $z \sim 0$ galaxies. Depending on which conditions evolve and the magnitude of that evolution, the relation between emission-line ratios and metallicity may change with redshift, potentially rendering current strong-line calibrations significantly biased at high redshifts.

Unbiased metallicity estimates for high-redshift galaxies based on the direct method are needed to evaluate the applicability of local metallicity calibrations at high redshift. However, due to the weakness of [O III]λ4363 and the

* Based on data obtained at the W.M. Keck Observatory, which is operated as a scientific partnership among the California Institute of Technology, the University of California, and NASA, and was made possible by the generous financial support of the W.M. Keck Foundation.
[6] Alfred P. Sloan Fellow.

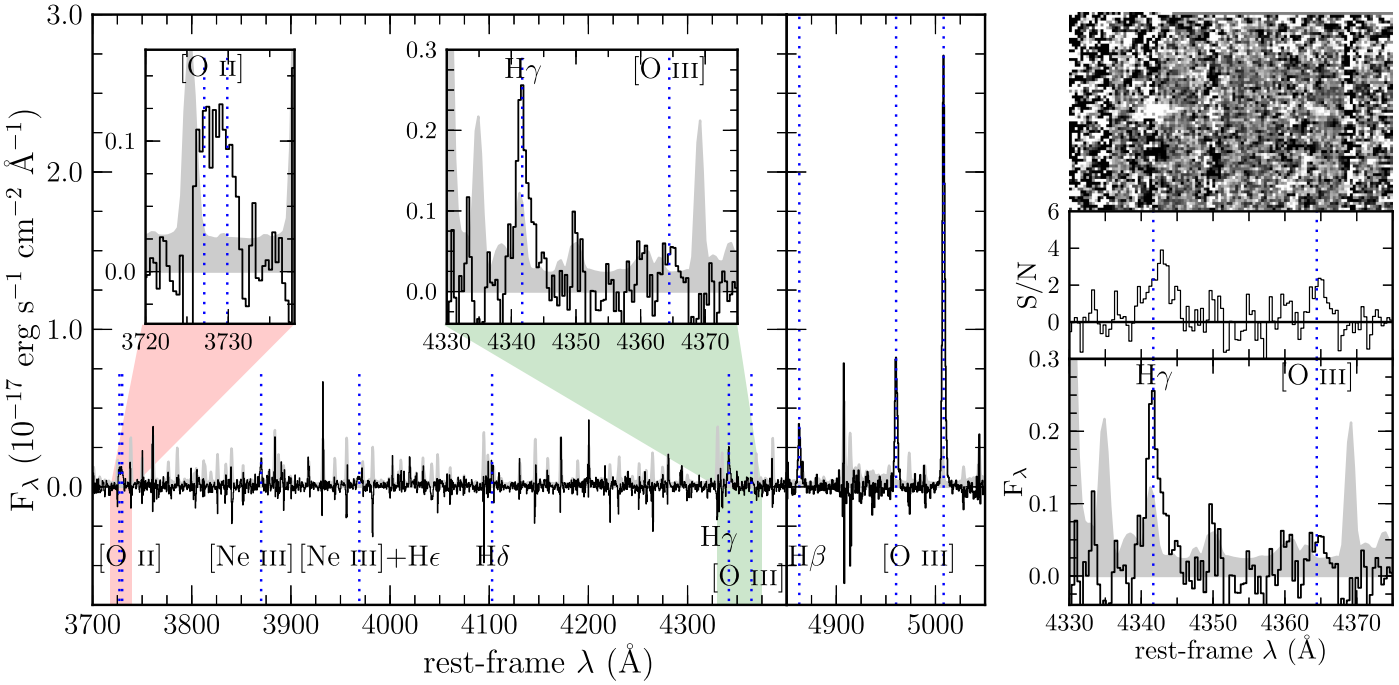

Figure 1. Spectrum of COSMOS-1908. Left: H- and K-band spectra of COSMOS-1908. The gray shaded region displays the magnitude of the error spectrum. Emission lines are labeled, and the spectral regions around [O II] and [O III]λ4363 are highlighted. Right: zoom-in of the wavelength region around Hγ and [O III] λ4363, showing the one-dimensional spectrum (bottom), signal-to-noise ratio spectrum (middle), and two-dimensional spectrum (top).

difficulties of observing in the near-infrared, this line has only been detected in 7 galaxies at $z > 1$ (Yuan & Kewley 2009; Brammer et al. 2012; Christensen et al. 2012; Stark et al. 2013; James et al. 2014; Maseda et al. 2014), most of which are gravitationally lensed, and has not been detected at $z > 1.9$. The small, inhomogeneous sample of direct-method metallicities at $z > 1$ has made it difficult to assess the state of metallicity calibrations at high redshifts.

In this Letter, we present observations of COSMOS-1908, an unlensed star-forming galaxy at $z = 3.08$ with a detection of [O III]λ4363, observed as part of the MOSFIRE Deep Evolution Field (MOSDEF) survey (Kriek et al. 2015). We investigate the physical conditions of nebular gas in COSMOS-1908, considering multiple emission lines to evaluate the utility of locally calibrated strong-line metallicity relations at $z \sim 3$. In Section 2, we present details about the observations and data reduction. We describe measurements of the spectral features in Section 3. In Section 4, we derive galaxy and ionized gas properties of COSMOS-1908. Finally, we discuss the implications of our results in Section 5. Throughout this Letter, the term "metallicity" refers to the gas-phase oxygen abundance (12+log(O/H)). We adopt a Λ-CDM cosmology with $H_0 = 70$ km s^{-1} Mpc^{-1}, $\Omega_m = 0.3$, and $\Omega_\Lambda = 0.7$.

2. OBSERVATIONS AND REDUCTION

We utilized data from the MOSDEF survey, described in detail in Kriek et al. (2015). The data were obtained on 2012 December 23 and 2013 April 1 using the MOSFIRE spectrograph (McLean et al. 2012) on the 10 m Keck I telescope. COSMOS-1908 was observed in the H and K bands on a MOSFIRE mask with 0.″7 wide slits, resulting in spectral resolutions of ~3650 and ~3600 in H and K, respectively. Individual exposures were 120 s in H and 180 s in K. The mask was observed for 72 minutes in H and 144 minutes in K using an ABBA dither pattern with a 1.″2 nod in December, and 64 minutes in H using an ABA′B′ dither pattern with 1.″5 and 1.″2 outer and inner nods in April. The total integration time was 136 minutes in H and 144 minutes in K.

The data were reduced using a custom IDL pipeline that produces a two-dimensional science and error spectrum for each slit on the mask that has been flat-fielded, sky-subtracted, cleaned of cosmic rays, wavelength-calibrated, and flux-calibrated (Kriek et al. 2015). One-dimensional science and error spectra were optimally extracted from the two-dimensional spectra. Science spectra were corrected for slit losses on an individual basis using *Hubble Space Telescope* (*HST*) F160W images and the average seeing for each filter. Emission-line fluxes were measured by fitting Gaussian profiles to the one-dimensional science spectrum. Uncertainties on line fluxes and all derived and measured quantities were estimated using a Monte Carlo technique, where the 1σ uncertainty bounds were taken to be the 16th and 84th percentile of the cumulative distribution function for each value.

In addition to our MOSFIRE observations, we utilized extensive multiwavelength photometric data that are available in the COSMOS field. COSMOS-1908 has coverage in 44 broad-, medium-, and intermediate-band filters from optical to infrared (rest-UV to rest-NIR), assembled by the 3D-HST team (Skelton et al. 2014; Momcheva et al. 2015).

3. THE DETECTION OF AURORAL [O III]λ4363

Deep observations with MOSFIRE allow us to identify several emission lines in the H- and K-band spectra of COSMOS-1908, presented in Figure 1. We measure a nebular redshift of $z = 3.0768$ using the best-fit centroid of [O III] λ5007, the line with the highest signal-to-noise ratio (S/N). In addition to the strong rest-optical lines [O III]$\lambda\lambda$4959, 5007, Hβ, and [O II]$\lambda\lambda$3726, 3729, there are many weak emission

Table 1
Properties of COSMOS-1908

Observed Emission-line Fluxes		
Line	Flux $\left(10^{-17}\frac{\text{erg}}{\text{s cm}^2}\right)$	Uncertainty $\left(10^{-17}\frac{\text{erg}}{\text{s cm}^2}\right)$
[O II]λ3726	1.09	0.19
[O II]λ3729	1.09	0.18
[Ne III]λ3869	1.84	0.21
Hδ	1.49	0.32
Hγ	2.21	0.34
[O III]λ4363	0.56	0.14
Hβ	4.72	0.25
[O III]λ4959	10.8	0.28
[O III]λ5007	33.3	0.70

Galaxy Properties	
Property	Value
R.A. (J2000)	$10^{\rm h}\,00^{\rm m}\,23\overset{\rm s}{.}36$
Decl. (J2000)	02°11′55″.9
z	3.0768
$\log(M_*/M_\odot)$	$9.33^{+0.18}_{-0.17}$
$E(B-V)_{\rm gas}$	$0.0^{+0.14}_{-0.0}$
SFR ($M_\odot$ yr^{-1})	49^{+30}_{-3}
sSFR (Gyr^{-1})	23^{+23}_{-6}
Area (kpc^2)	4.4
$\Sigma_{\rm SFR}$ ($M_\odot$ yr^{-1} kpc^{-2})	11^{+7}_{-1}
n_e (cm^{-3})	520^{+600}_{-400}
T_e([O III]) (K)	14000^{+1950}_{-1400}
T_e([O II]) (K)	12800^{+1350}_{-1000}
12+log(O$^+$/H$^+$)	$6.87^{+0.17}_{-0.14}$
12+log(O^{++}/H$^+$)	$7.96^{+0.13}_{-0.14}$
12+log(O/H)	$8.00^{+0.13}_{-0.14}$

lines detected in the H-band. These include [Ne III]λ3869, [Ne III]λ3968 blended with Hϵ, Hδ, Hγ, and [O III]λ4363. The observed emission-line fluxes and uncertainties are presented in Table 1. COSMOS-1908 displays a high level of excitation and ionization based on the strength of [Ne III] and the large [O III] λ5007 flux compared to that of Hβ and [O II].

The auroral [O III]λ4363 line is detected with a formal significance of 4.0σ. The redshift of COSMOS-1908 fortuitously places [O III]λ4363 in a wavelength region that is free of skylines. The centroid of [O III]λ4363 implies a redshift (z = 3.0769) that closely matches the one measured from stronger lines. Additionally, emission can be seen at the expected location of [O III]λ4363 in the two-dimensional spectrum (Figure 1, right), and the S/N spectrum shows a coherent peak centered at the expected location of the line, where seven consecutive pixels have S/N > 1. We conclude that [O III]λ4363 is real and significantly detected, making COSMOS-1908 the highest-redshift galaxy for which [O III] λ4363 has been detected.

4. PROPERTIES OF COSMOS-1908

4.1. The Stellar Content of COSMOS-1908

We estimate the stellar mass of COSMOS-1908 via spectral energy distribution (SED) fitting. The photometry is shown in Figure 2. There is a clear excess in the K-band photometry due to emission-line flux from [O III]+Hβ on top of the stellar continuum, as well as a probable excess in the H-band from weaker lines. For this reason, we exclude the H- and K-band photometric points when fitting the SED. The intermediate-band photometry at 5050 and 7670 Å were also excluded from the fit because of contributions from strong Lyα and C III] λ1909 emission, respectively. COSMOS-1908 additionally displays excess flux blueward of the Balmer break in the J-band, which may be due to nebular continuum emission indicative of a young stellar population (Reines et al. 2010). Since our models are not tuned to fit nebular continuum emission, we exclude the J-band photometry as well. The remaining photometry was fit using the SED-fitting code FAST (Kriek et al. 2009), with the Conroy et al. (2009) stellar population synthesis models, assuming a Chabrier (2003) initial mass function, a delayed-τ star formation history (SFR $\propto te^{-t/\tau}$), and the Calzetti et al. (2000) attenuation curve. We assume a stellar metallicity of 0.16 $Z_\odot$, the closest metallicity in the library of models to the measured gas-phase metallicity for COSMOS-1908 (see Section 4.5). The photometry and best-fit SED model are shown in the left panel of Figure 2. The best-fit age of the stellar population is $t = 160^{+200}_{-110}$ Myr with an e-folding time of τ = 10 Gyr, indicating a rising star formation history. The extinction of the stellar continuum in the best-fit model is $E(B-V)_{\rm stars} = 0.12^{+0.03}_{-0.05}$. The stellar mass is found to be $\log(M_*/M_\odot) = 9.33^{+0.18}_{-0.17}$. Fitting including H- and K-band photometry that have been corrected for emission-line contamination using measured line fluxes changes $E(B-V)_{\rm stars}$ by <0.05, age by $\lesssim$100 Myr, and stellar mass by <0.2 dex.

The right panel of Figure 2 shows *HST* postage stamp images of COSMOS-1908 in the F160W (rest-optical) and F606W (rest-UV) filters. The galaxy displays a compact morphology that is slightly elongated toward the south. Using the F606W image, we measure a rest-UV area of 4.4 kpc^2 from the number of pixels that are 2σ or more above the background noise. It is unlikely that COSMOS-1908 is dominated by ionization from an active galactic nucleus due to its low stellar mass and the lack of a strong brightness peak in the central region.

4.2. Nebular Extinction and Star Formation Rate

The reddening of nebular emission lines can significantly affect the inferred star formation rate (SFR), line ratios, and derived metallicities. The amount of nebular extinction can be estimated using ratios of hydrogen Balmer-series lines. Balmer-series line fluxes are first corrected for stellar absorption using the best-fit SED model. Due to the strength of the emission lines, this correction is small, only 0.7%, 2%, and 3.5% for Hβ, Hγ, and Hδ, respectively. Nebular reddening is estimated using Balmer-series line ratios, assuming intrinsic ratios of Hγ/H β = 0.468 and Hδ/H β = 0.259 (Osterbrock & Ferland 2006) and the extinction curve of Cardelli et al. (1989). The observed Balmer ratios of COSMOS-1908 are consistent with no reddening; $E(B-V)_{\rm gas} = 0.0^{+0.14}_{-0.0}$, an upper limit that is consistent within the uncertainties with the stellar reddening. The SFR is estimated from Hβ using the relation of Kennicutt (1998) converted to a Chabrier (2003) IMF, assuming an intrinsic ratio of Hα/Hβ = 2.847 (Osterbrock & Ferland 2006). COSMOS-1908 is vigorously forming stars, with SFR $= 49^{+30}_{-3}$ $M_\odot$ yr^{-1}, specific SFR (sSFR; SFR/M_*) of 23^{+23}_{-6} Gyr^{-1}, and SFR surface density ($\Sigma_{\rm SFR}$; SFR/Area) of 11^{+7}_{-1} $M_\odot$ yr^{-1} kpc^{-2}.

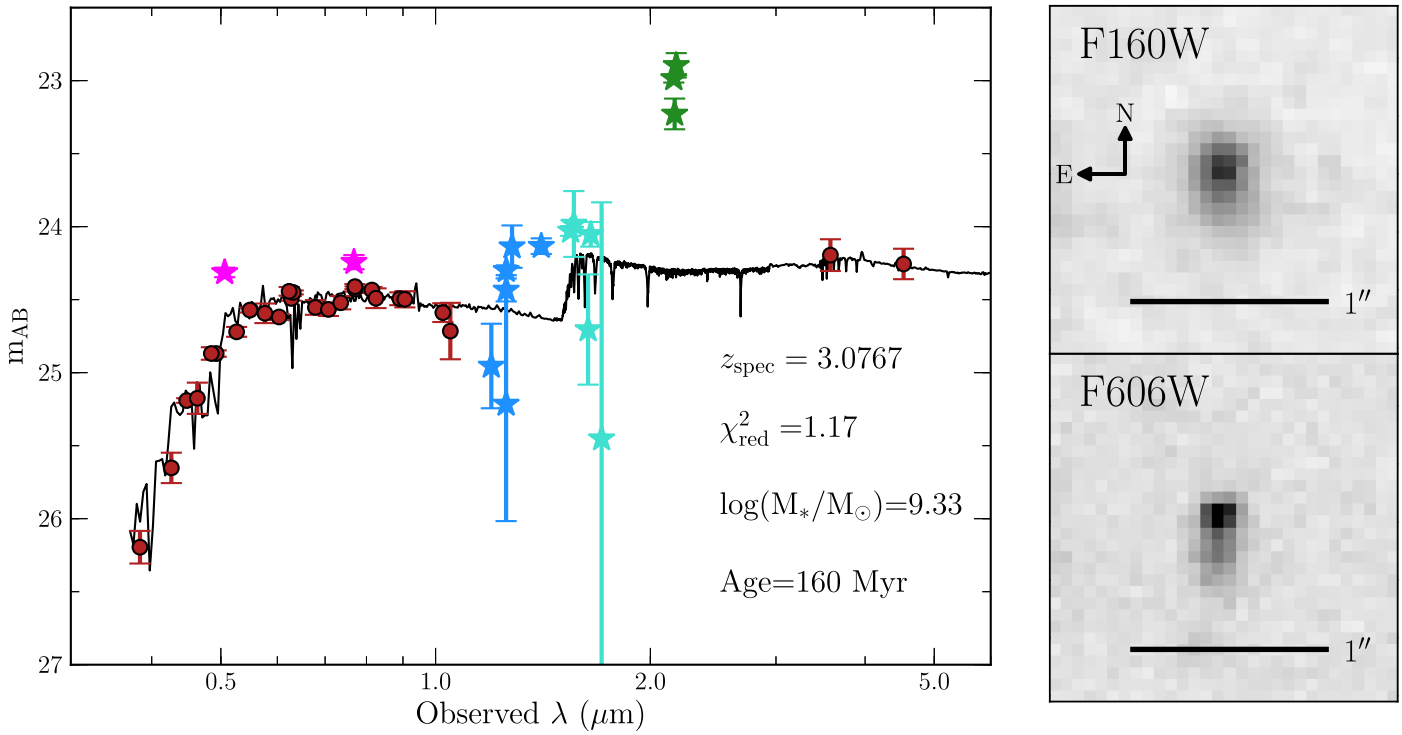

Figure 2. Left: observed photometry and best-fit SED model for COSMOS-1908. The red circles indicate photometry used for SED fitting. Stars denote photometry excluded from the SED fitting process due to contamination. Bands removed are: IA505 and IA767 (magenta), J (blue), H (cyan), and K (green). The 3D-HST photometric catalog includes multiple overlapping filters in the J, H, and K bands. Right: postage stamp images of COSMOS-1908 in the F160W and F606W filters. Images are 1.″5 on a side, and the plate scale is 0.″06/pixel.

The galaxy properties of COSMOS-1908 are presented in Table 1.

4.3. [O III] λ 5007 Equivalent Width

We measure a large [O III]λ5007 rest-frame equivalent width of EW([O III]) = 1600 Å using the continuum level from the best-fit SED model. Objects with EW([O III]) > 1000 Å are extremely rare at $z \lesssim 2.3$ (Atek et al. 2011), but appear to be common at $z \sim 6$–7 (Smit et al. 2014). Observing an object with such a high EW in the small survey volume of the MOSDEF $z > 3$ observations suggests a significant increase in the occurrence rate of high-EW galaxies from $z \sim 2$ to $z \sim 3$. Analysis of objects like COSMOS-1908 can provide insight into the nature of $z \sim 7$ star-forming galaxies with similar nebular EWs. COSMOS-1908 displays similar properties to the Lyman-continuum leaking galaxy Ion2 at $z = 3.2$ (de Barros et al. 2016), including EW([O III])>1000 Å and [O III]λ5007/[O II]λ3727 > 10, and may be a good candidate for Lyman-continuum detection.

4.4. Electron Density

The electron density serves as a robust proxy for the hydrogen gas density in H II regions and can affect the strength of collisionally excited lines. We calculate the electron density using the [O II]λ3729/λ3726 ratio (roughly unity) and the IRAF routine NEBULAR.TEMDEN (Shaw & Dufour 1994) with updated O II atomic data following Sanders et al. (2016). We assume an electron temperature of 12,800 K, the estimated T_e([O II]) for COSMOS-1908 (see Section 4.5). We find the electron density to be $n_e = 520^{+600}_{-400}$ cm^{-3}. This high electron density compared to those of local star-forming galaxies and H II regions is in agreement with the order-of-magnitude increase in electron density from $z \sim 0$ to $z \sim 2.3$ observed in Sanders et al. (2016).

4.5. Electron Temperature and Oxygen Abundance

We estimate the oxygen abundance following the prescription of Izotov et al. (2006). The relative population of oxygen in ionization states higher than O^{++} is assumed to be negligible, such that the total oxygen abundance is

$$\frac{O}{H} \approx \frac{O^+}{H^+} + \frac{O^{++}}{H^+}. \quad (1)$$

The analytic equations of Izotov et al. (2006) for O^+/H^+ and O^{++}/H^+ require knowledge of the electron density, electron temperatures in the O^+ and O^{++} zones, and dust-corrected emission-line fluxes for [O II], Hβ, and [O III].

We calculate T_e([O III]) using NEBULAR.TEMDEN with updated O III collision strengths from Storey et al. (2014) and transition probabilities from the NIST MCHF database (Fischer & Tachiev 2014). In the density regime $n_e \lesssim 1000$ cm^{-3}, T_e is insensitive to changes in density, so we do not iteratively solve for n_e and T_e simultaneously. For COSMOS-1908, we find [O III]λλ4959, 5007/λ4363 = $80.0^{+23.1}_{-20.0}$, which corresponds to an electron temperature in the O^{++} zone of T_e([O III]) = $14{,}000^{+1950}_{-1400}$ K. We do not have wavelength coverage of the auroral [O II]λλ7320, 7330 lines to determine T_e([O II]) directly. Instead, we assume the linear T_e([O III])–T_e([O II]) relation of Campbell et al. (1986). We find an electron temperature in the O^+ zone of T_e([O II]) = $12{,}800^{+1350}_{-1000}$ K. The total oxygen abundance of COSMOS-1908 is found to be $12 + \log(O/H) = 8.00^{+0.13}_{-0.14}$ (0.2 $Z_\odot$; Asplund et al. 2009). The

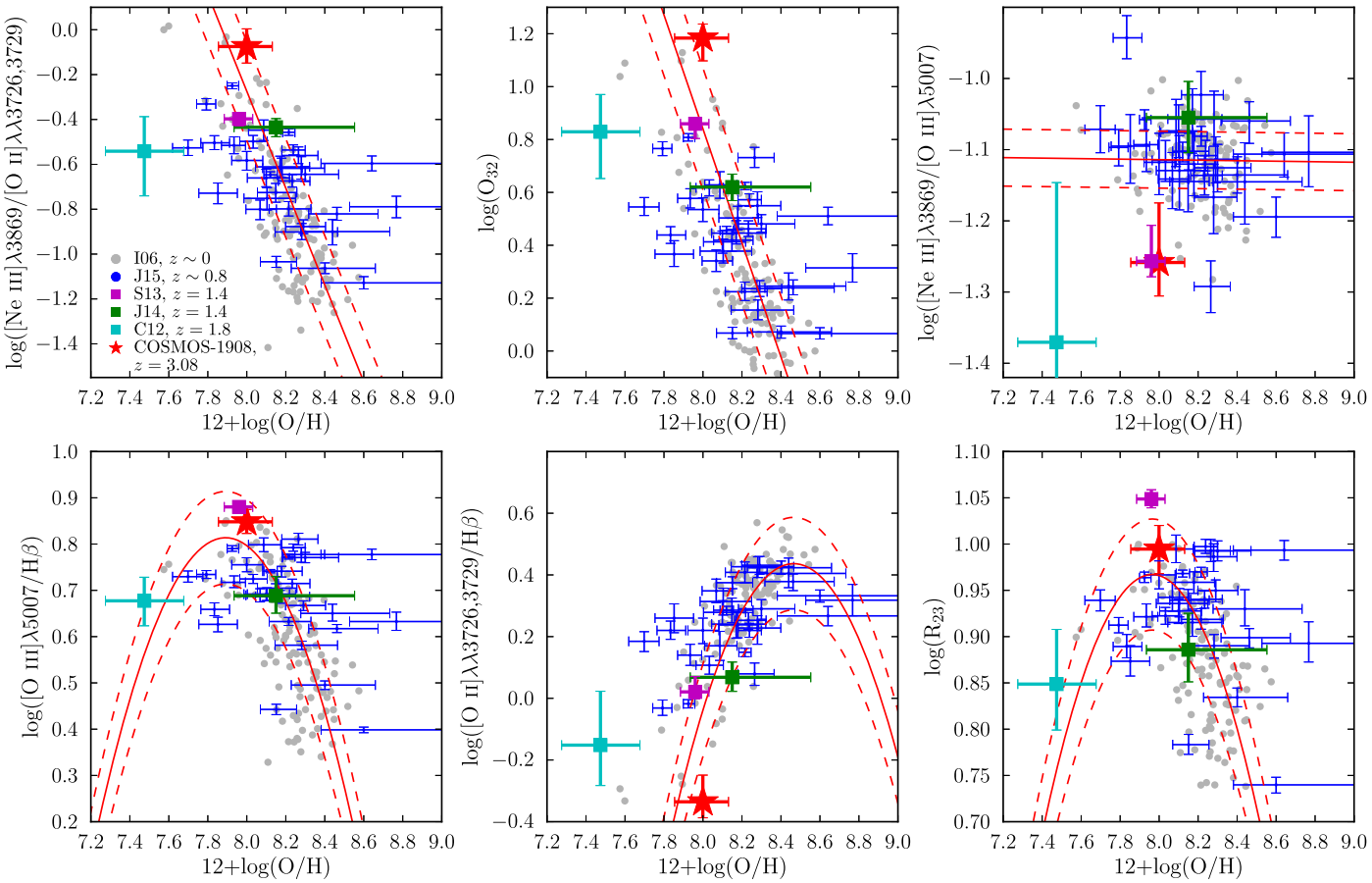

Figure 3. Emission-line ratios vs. direct-method oxygen abundance for COSMOS-1908 and lower-redshift comparison samples. In each panel, the red star indicates COSMOS-1908. Gray points show the $z \sim 0$ sample from (Izotov et al. 2006, I06), while blue error bars show the positions of $z \sim 0.8$ galaxies from Jones et al. (2015, J15). The red solid and dashed lines display the best-fit relations to the $z \sim 0$ sample and 1σ scatter (Jones et al. 2015), offset +0.045 dex in 12+log(O/H) to account for the different T_e([O III])–T_e([O II]) relation and O III atomic data used in this study. The magenta, green, and cyan squares show the $z = 1.4$ galaxy from Stark et al. (2013, S13) and Mainali et al. (2016, in preparation), the $z \sim 1.4$ galaxy from James et al. (2014, J14), and the $z \sim 1.8$ galaxy from Christensen et al. (2012, C12), respectively.

oxygen abundance, ionic abundances, electron temperatures, and density are listed in Table 1.

5. DISCUSSION

We investigate the evolution in the relationship between emission-line ratios and metallicity by comparing COSMOS-1908 to galaxies at lower redshifts with abundance determinations based on [O III]λ4363. Recently, Jones et al. (2015) found that relations between direct-method oxygen abundance and ratios of neon, oxygen, and hydrogen emission lines do not evolve from $z = 0 - 1$, using a sample of 32 star-forming galaxies at $z \sim 0.8$ from the DEEP2 Galaxy Redshift Survey (Newman et al. 2013). We perform a similar comparison using galaxies at higher redshifts. The low-redshift comparison sample includes the $z \sim 0.8$ galaxies from Jones et al. (2015) and 126 star-forming galaxies at $z \sim 0$ from Izotov et al. (2006) that have spectral coverage of [O II]. We additionally compare to three galaxies at $z \sim 1.5$ (Christensen et al. 2012; Stark et al. 2013; James et al. 2014, Mainali et al. 2016, in preparation). All galaxies in the comparison samples have detections of [O III]λ4363, and reddening corrections and oxygen abundances recalculated with the methods described in Section 4. Uncertainties on emission-line ratios are calculated using a Monte Carlo technique, and include uncertainties in measurement and reddening correction.

The emission-line ratios and oxygen abundances are shown in Figure 3. The line ratios displayed in each panel are sensitive to O/H, with the exception of [Ne III]/[O III], which should remain approximately constant with metallicity because it is a ratio of similar ionization states of α-capture elements. In all five panels with metallicity-sensitive line ratios, COSMOS-1908 is consistent with the local best-fit relations within the uncertainties and intrinsic scatter. There are few galaxies in the low-redshift comparison samples that have the levels of low-metallicity and high-excitation that COSMOS-1908 displays, so this result relies on a small level of extrapolation of the $z \sim 0$ relations. Of the four galaxies at $z > 1$, COSMOS-1908 lies slightly toward the high-excitation side of the local relations, the Stark et al. (2013) and James et al. (2014) galaxies fall very nearly on each local relation, and the Christensen et al. (2012) galaxy lies toward the low-excitation side. Collectively, galaxies at $z > 1$ do not show a systematic offset toward higher excitation at fixed metallicity, and the relation between these line ratios and O/H does not strongly evolve.

The close proximity of COSMOS-1908 to the local relations implies that evolution of the ionization parameter or ionizing spectrum at fixed O/H is small, if present. It has been

suggested that high-redshift galaxies may have higher ionization parameters than local galaxies because of a scaling up of the radiation field due to more concentrated star formation (Kewley et al. 2015; Cullen et al. 2016; Kashino et al. 2016). This scenario predicts that COSMOS-1908 should have a much higher ionization parameter than local galaxies at similar O/H due to its extreme sSFR and $\Sigma_{\rm SFR}$, which would be observed as large offsets in [O III]/[O II], [O III]/Hβ, and [Ne III]/[O II] at fixed O/H. The models presented in Cullen et al. (2016) predict that [O III]/Hβ at fixed metallicity will be >0.1 dex larger at $z = 3.1$ due to an increase in ionization parameter at fixed O/H. Such offsets are not observed in Figure 3.

Our results instead suggest a scenario in which high-redshift and $z \sim 0$ galaxies have similar ionization parameters at fixed metallicity, while high-redshift galaxies have higher ionization parameters than local galaxies at fixed M_* due to the evolution of the MZR. This scenario is consistent with our earlier findings in Sanders et al. (2016) using a sample of ∼100 star-forming galaxies at $z \sim 2.3$ from the MOSDEF survey. The properties of COSMOS-1908 and the $z \sim 1.5$ and $z \sim 0.8$ comparison samples suggest that the same relationship between metallicity and ionization parameter holds out to $z \sim 3$. Since changes in electron density minimally affect line ratios at subsolar metallicities (Sanders et al. 2016), the agreement of the high- and low-redshift samples in Figure 3 implies that strong-line metallicity calibrations using only lines of oxygen, neon, and hydrogen can reliably predict abundances from $z \sim 0$ to $z \sim 3$.

Currently, these results are based upon a handful of galaxies at $z \sim$ 1–3.5, which is not sufficient to statistically constrain the behavior of the entire galaxy population at high redshifts. More detections of [O III]λ4363 for high-redshift galaxies are required to gain a complete understanding of the behavior of metallicity indicators at $z > 1$. One way forward is selecting objects similar to COSMOS-1908 from photometric surveys by identifying objects with large excess flux in the photometric band covering [O III]$\lambda\lambda$4959, 5007, suggestive of a large [O III] equivalent width and low metallicity. Such objects are good candidates for [O III]λ4363 detection in deep spectroscopic observations. Detections of weak features such as [O III]λ4363 for large samples at high redshift will be enabled by the next-generation near-infrared facilities such as the *James Webb Space Telescope* and Thirty Meter Telescope.

We would like to thank Tucker Jones, Dan Stark, and Ramesh Mainali for providing data used in this study. We acknowledge support from NSF AAG grants AST-1312780, 1312547, 1312764, and 1313171, and archival grant AR-13907, provided by NASA through the Space Telescope Science Institute. We wish to extend special thanks to those of Hawaiian ancestry on whose sacred mountain we are privileged to be guests. Without their generous hospitality, most of the observations presented herein would not have been possible.

REFERENCES

Andrews, B. H., & Martini, P. 2013, ApJ, 765, 140
Asplund, M., Grevesse, N., Sauval, A. J., & Scott, P. 2009, ARA&A, 47, 481
Atek, H., Siana, B., Scarlata, C., et al. 2011, ApJ, 743, 121
Brammer, G. B., Sánchez-Janssen, R., Labbé, I., et al. 2012, ApJL, 758, L17
Calzetti, D., Armus, L., Bohlin, R. C., et al. 2000, ApJ, 533, 682
Campbell, A., Terlevich, R., & Melnick, J. 1986, MNRAS, 223, 811
Cardelli, J. A., Clayton, G. C., & Mathis, J. S. 1989, ApJ, 345, 245
Chabrier, G. 2003, PASP, 115, 763
Christensen, L., Laursen, P., Richard, J., et al. 2012, MNRAS, 427, 1973
Conroy, C., Gunn, J. E., & White, M. 2009, ApJ, 699, 486
Cullen, F., Cirasuolo, M., Kewley, L. J., et al. 2016, arXiv:1605.04228
de Barros, S., Vanzella, E., Amorín, R., et al. 2016, A&A, 585, A51
Erb, D. K., Shapley, A. E., Pettini, M., et al. 2006, ApJ, 644, 813
Fischer, C. F., & Tachiev, G. 2014, MCHF/MCDHF Collection, Version 2, Ref No. 10 & 20, Available online at http://physics.nist.gov/mchf, National Institude of Standards and Technology
Izotov, Y. I., Stasińska, G., Meynet, G., Guseva, N. G., & Thuan, T. X. 2006, A&A, 448, 955
James, B. L., Pettini, M., Christensen, L., et al. 2014, MNRAS, 440, 1794
Jones, T., Martin, C., & Cooper, M. C. 2015, ApJ, 813, 126
Kashino, D., Silverman, J. D., Sanders, D., et al. 2016, arXiv:1604.06802
Kennicutt, R. C., Jr. 1998, ARA&A, 36, 189
Kewley, L. J., Dopita, M. A., Leitherer, C., et al. 2013, ApJ, 774, 100
Kewley, L. J., Zahid, H. J., Geller, M. J., et al. 2015, ApJL, 812, L20
Kriek, M., Shapley, A. E., Reddy, N. A., et al. 2015, ApJS, 218, 15
Kriek, M., van Dokkum, P. G., Labbé, I., et al. 2009, ApJ, 700, 221
Mainali, R., et al. 2016, in preparation
Marino, R. A., Rosales-Ortega, F. F., Sánchez, S. F., et al. 2013, A&A, 559, A114
Maseda, M. V., van der Wel, A., Rix, H.-W., et al. 2014, ApJ, 791, 17
Masters, D., McCarthy, P., Siana, B., et al. 2014, ApJ, 785, 153
McLean, I. S., Steidel, C. C., Epps, H. W., et al. 2012, Proc. SPIE, 8446, 84460J
Momcheva, I. G., Brammer, G. B., van Dokkum, P. G., et al. 2015, arXiv:1510.02106
Newman, J. A., Cooper, M. C., Davis, M., et al. 2013, ApJS, 208, 5
Onodera, M., Carollo, C. M., Lilly, S., et al. 2016, ApJ, 822, 42
Osterbrock, D. E., & Ferland, G. J. 2006, Astrophysics of Gaseous Nebulae and Active Galactic Nuclei (Sausalito, CA: Univ. Science Books)
Pettini, M., & Pagel, B. E. J. 2004, MNRAS, 348, L59
Pilyugin, L. S., & Thuan, T. X. 2005, ApJ, 631, 231
Reines, A. E., Nidever, D. L., Whelan, D. G., & Johnson, K. E. 2010, ApJ, 708, 26
Sanders, R. L., Shapley, A. E., Kriek, M., et al. 2015, ApJ, 799, 138
Sanders, R. L., Shapley, A. E., Kriek, M., et al. 2016, ApJ, 816, 23
Shapley, A. E., Reddy, N. A., Kriek, M., et al. 2015, ApJ, 801, 88
Shaw, R. A., & Dufour, R. J. 1994, in ASP Conf. Ser. 61, Astronomical Data Analysis Software and Systems III, ed. D. R. Crabtree, R. J. Hanisch, & J. Barnes (San Francisco, CA: ASP), 327
Skelton, R. E., Whitaker, K. E., Momcheva, I. G., et al. 2014, ApJS, 214, 24
Smit, R., Bouwens, R. J., Labbé, I., et al. 2014, ApJ, 784, 58
Stark, D. P., Auger, M., Belokurov, V., et al. 2013, MNRAS, 436, 1040
Steidel, C. C., Rudie, G. C., Strom, A. L., et al. 2014, ApJ, 795, 165
Storey, P. J., Sochi, T., & Badnell, N. R. 2014, MNRAS, 441, 3028
Tremonti, C. A., Heckman, T. M., Kauffmann, G., et al. 2004, ApJ, 613, 898
Troncoso, P., Maiolino, R., Sommariva, V., et al. 2014, A&A, 563, A58
Yuan, T.-T., & Kewley, L. J. 2009, ApJL, 699, L161